Determination of the absolute configurations of bicyclo[3.1.0]hexane derivatives *via* electronic circular dichroism, optical rotation dispersion and vibrational circular dichroism spectroscopy and density functional theory calculations†

Guochun Yang, Jing Li, Yang Liu, Todd L. Lowary and Yunjie Xu*

Received 17th February 2010, Accepted 26th May 2010
First published as an Advance Article on the web 22nd June 2010
DOI: 10.1039/c002655g

The electronic circular dichroism (ECD), optical rotation dispersion (ORD), and vibrational circular dichroism (VCD) spectra of a pair of enantiomers, *i.e.* **3** and **4**, of a bicyclo[3.1.0]hexane derivative have been measured in acetonitrile and acetonitrile-d_3, respectively. Extensive conformational searches at the B3LYP/6-311++G** level have been carried out for **3**, which has four OH and one N_3 functional groups. For the bicyclo[3.1.0]hexane ring of **3**, the *boat*-like conformers have been found to be much more stable than the *chair*-like conformers, while the number and the strength of the intramolecular hydrogen bonds have been identified as the dominant factors in the relative stability among the *boat*-like and among the *chair*-like conformers. DFT simulations of the ECD, ORD and VCD spectra have been performed for all low energy conformers at the B3LYP/6-311++G** and B3LYP/aug-cc-pVDZ level. Implicit continuum polarization model has been used to account for solvent effects in all these chiroptical measurements. Comparison of the DFT simulations with the experimental data shows that all three chiroptical properties yield the same absolute configuration assignment for **3**. This work demonstrates that using multiple chiroptical spectroscopic methods in combination with DFT calculations allows one to determine absolute configurations with high confidence for chiral carbohydrates and their analogues, which possess a large number of rotatable bonds.

1. Introduction

Mycobacteria, including the human pathogens *Mycobacterium tuberculosis* and *Mycobacterium leprae*, possess an extraordinarily thick and complicated cell wall structure.[1] A key structural component of this cell wall is a glycoconjugate, arabinogalactan, which contains galactofuranose and arabinofuranose residues, and monosaccharides that are xenobiotic to mammalian biology. The arabinogalactan is essential for the survival of the mycobacteria and, hence, the glycosyltransferases that are involved in the synthesis of this furanose-containing glycan are ideal targets for drug action as novel antituberculosis agents.[2] An important structural characteristic of furanose rings is their inherent flexibility.[3] It is well known that the conformational preference of the furanose ring influences the biological activity of molecules containing them.[4] Over the past few years, much effort has been devoted to synthetic and conformational investigations aimed at the development of inhibitors of mycobacterial glycosyltransferases[5] and as part of those studies conformationally restricted furanose analogs have been explored.[5c]

Compounds **1** and **2** (Chart 1) have been synthesized as a conformationally-restricted mimic of the arabinofuranose and galactofuranose rings, respectively, and are precursors to potential inhibitors of mycobacterial glycosyltransferases.[5c] In the synthesis of these compounds, one step required the differentiation of a pair of enantiomers, **3** and **4** (Chart 1), which are key intermediates generated from a single starting material. The absolute configurations (ACs) of **3** and **4** were indirectly inferred from the X-ray single crystal analysis of a crystalline 2,4-dinitrophenylhydrazone derivative of **1**.[5d] Obtaining a single crystal for X-ray crystallography can be time consuming and often it is necessary to prepare a derivative of the compound of interest to provide a crystalline material. One concern is that derivatization process may introduce uncertainty into the AC determination through epimerization of stereocentres in the original sample. It is therefore highly desirable

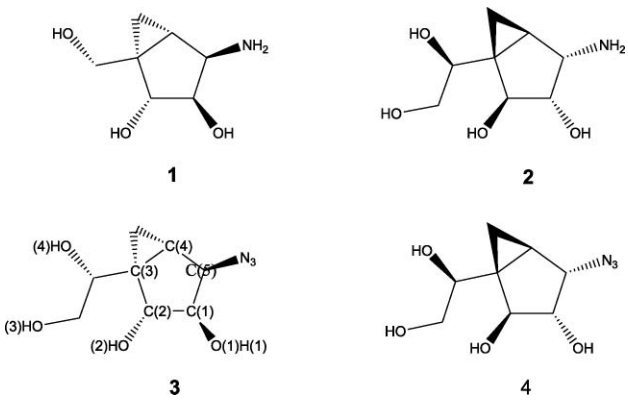

Chart 1

Department of Chemistry and Alberta Ingenuity Centre for Carbohydrate Science, University of Alberta, Edmonton, AB, Canada T6G 2G2. E-mail: yunjie.xu@ualberta.ca; Tel: +1-780-492-1244

† Electronic supplementary information (ESI) available: Supplementary tables and figures. See DOI: 10.1039/c002655g

to have a convenient and reliable technique where one can use the original sample directly.

Thanks to recent advances in experimental techniques and, in particular, computational methods in electronic circular dichroism (ECD), optical rotation dispersion (ORD), and vibrational circular dichroism (VCD) spectroscopy, AC determinations using one or a combination of these chiroptical techniques have become well accepted.[6] The number of organic compounds whose ACs were determined by using these chiroptical techniques has increased significantly in the last few years. On the other hand, for carbohydrates and their analogues, this number remains extremely small.[7] This is due largely to the fact that they often have many OH functional groups and many degrees of conformational freedom, and are therefore very difficult to model theoretically in order to achieve reliable AC assignments. A number of recent studies show that using more than one chiroptical spectroscopic methods for the determination of the ACs of chiral molecules usually provides more reliable answers.[8] In this paper, we report the concerted applications of the ECD, ORD, and VCD chiroptical techniques combined with DFT simulations to the determination of the ACs of **3** and **4**.

Results and Discussion

To assign the ACs of **3** and **4** based on the experimental ECD, ORD, and VCD spectral measurements, extensive theoretical simulations were performed to simulate their chiroptical quantities in solution. In the following discussion, we describe geometry searches of all possible low energy intramolecular hydrogen (H)-bonded conformers, and the related ECD, ORD, and VCD spectral simulations under both gas phase and solution phase conditions. The experimental ECD and ORD, as well as VCD spectra, show that **3** and **4** are a pair of enantiomers (*vide infra*). For simplicity, we use **3** as the example molecule throughout our discussions unless otherwise indicated.

Conformational Analysis

Before moving on to discuss various chiroptical properties of **3**, we first present the searches for the dominant conformational structures of **3**. Compound **3** has many rotatable bonds, and the bicyclo[3.1.0]hexane ring can undergo deformation. Because **3** contains four hydroxyl (OH) and one azide (N_3) functional group, one can expect intramolecular H-bonds formed between these functional groups. For example, H-bonding between two OH groups or between an OH group and one of the nitrogen atoms is possible. To find the most stable conformers of **3**, the following search strategy was used. First, we considered the possible ring conformations associated with bicyclo[3.1.0]hexane ring. Unlike most five-membered rings, the [3.1.0]-bicyclo-hexane ring is quite rigid due to the fusion of the cyclopropane and cyclopentane rings, and these bicylic species can adopt *boat*-like or *chair*-like conformations. The preference for the *boat*-like structures over the *chair*-like structures has been well documented.[9] Searches were therefore carried out to find the two different classes of conformers associated with the *boat*-like or *chair*-like bicyclo[3.1.0]hexane ring (Fig. 1). These two classes are labelled with capital letters: B for the *boat*-like form and C for the *chair*-like form in their names, respectively. The six hindered rotations depicted in Fig. 2

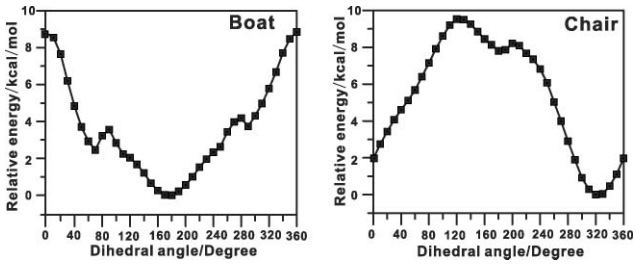

Fig. 1 The calculated potential energy profiles of the *boat*-like and *chair*-like forms for the rotation of H(1)–O(1) around the C(1)–O(1) bond as a function of the dihedral angle H(1)–O(1)–C(1)–C(5) at the DFT/B3LYP/6-31G* level of theory.

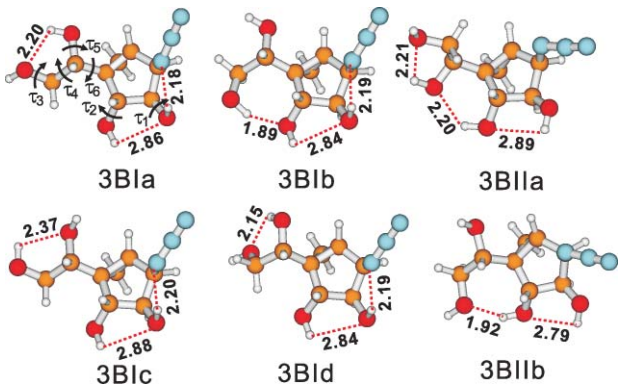

Fig. 2 Optimized geometries of the six most stable conformers of **3** at the B3LYP/6-311++G** level of theory. The important intramolecular H-bonds and the corresponding bond lengths (in Å) are indicated. The six rotatable bonds considered in the conformational searches are also indicated.

are governed by the formation of intramolecular H-bonds and steric hindrance. For these reasons, the rotation of one bond is often strongly coupled with another or several others. To allow us to systematically identify all possible low energy conformers, we chose to consider the rotation of the O(1)H(1) hydroxyl group around the C(1)–O(1) bond (Chart 1) in the second step. The potential energy surface cut scans (Fig. 1) of both the *boat*-like and *chair*-like forms have been performed for the dihedral angle (H(1)–O(1)–C(1)–C(5)) from 0° to 360° in 20° intervals. One can see from Fig. 1 that for the *boat*-like form, three minima exist, which correspond to the dihedral angles at about 60°, 180°, and 300°, labelled as **I**, **II** and **III**, respectively. Two minima exist about this bond in the *chair*-like form, which correspond to dihedral angles at roughly 180° and 320°, labelled as **I** and **II**, respectively. The guiding principle of the third geometry search was to form as many intramolecular H-bonds as possible by rotating the other five torsional angles (Fig. 2) to identify the lowest energy conformers.[10] We chose not to further separate the conformers found into different classes. Instead, we label them with letters, **a**, **b**, **c** and so on, based on their relative predicted stability.

In total, 40 structures were identified and their identification as true minima was confirmed with the subsequent harmonic frequency calculations. Only six of them with a Boltzmann factor > 1% are depicted in Fig. 2, while the rest are shown in Figure S1 in the ESI.† The important intramolecular H-bonds in these structures are also indicated in Fig. 2. Each geometry is labelled by three letters. For example, **B** in **BIa** indicates that

Table 1 The relative Gibbs free energies ΔG (kcal mol^{-1}), relative total energies ΔE (kcal mol^{-1}), and the normalized Boltzmann factors B_f (in%) at 298.15 K based on the relative total energies and the relative Gibbs free energies of the conformers of **3** at the B3LYP/6-311++G** level of theory

	ΔE	$B_f(\Delta E)$	ΔG	$B_f(\Delta G)$
3BIa	0.0	39.20	0.0	49.02
BIb	0.22	27.08	0.63	17.06
BIc	1.27	4.58	1.12	7.53
BId	2.02	1.29	1.97	1.76
BIe	2.54	0.53	2.60	0.60
BIf	3.01	0.24	2.80	0.44
BIg	3.28	0.15	3.11	0.26
BIh	3.45	0.12	2.92	0.36
BIi	3.50	0.11	3.29	0.19
BIj	3.85	0.06	3.86	0.07
BIIa	0.33	22.47	0.56	19.19
BIIb	2.05	1.23	2.29	1.03
BIIc	2.68	0.42	2.84	0.40
BIId	3.19	0.18	3.15	0.24
BIIe	3.31	0.15	3.27	0.20
BIIf	3.17	0.18	3.41	0.16
BIIg	3.06	0.22	3.43	0.15
BIIh	3.32	0.15	3.56	0.12
BIIi	3.17	0.24	3.75	0.11
BIIj	3.57	0.09	3.96	0.06
BIIIa	2.33	0.77	2.60	0.61
BIIIb	2.87	0.31	3.07	0.27
BIIIc	3.87	0.06	4.43	0.03
BIIId	4.30	0.03	4.45	0.03
BIIIe	4.79	0.01	4.88	0.01
3CIa	3.41	0.12	3.21	0.22
CIb	4.52	0.02	4.27	0.04
CIc	4.90	0.01	4.62	0.02
CId	4.95	0.01	4.62	0.03
CIe	4.76	0.01	4.79	0.02
CIf	6.08	0.0	5.27	0.01
CIg	5.67	0.0	5.52	0.01
CIh	5.75	0.0	5.65	0.0
CIi	6.47	0.0	6.15	0.0
CIj	7.02	0.0	6.61	0.0
CIIa	6.98	0.0	6.52	0.0
CIIb	8.71	0.0	8.07	0.0
CIIc	9.79	0.0	9.22	0.0
CIId	9.96	0.0	9.33	0.0
CIIe	10.94	0.0	10.63	0.0

the bicyclo[3.1.0]hexane ring exits in the *boat*-like form, while the second letter **I** specifies that the dihedral angle of H(1)–O(1)–C(1)–C(5) is roughly 60°, and the lower case letter **a** refers to the relative stability sequence in each class of conformers with **a** being the most stable one and **b** being the next most stable one and so on. To evaluate the effects of the OH conformations on that of the five-membered ring, the pseudorotational phase angles, as defined by the Altona-Sundaralingam system,[11] have been calculated for the six most stable conformers and are given in Table S1 in the ESI.† As one can see, these values differ very little—no more than six degrees with an average of 344 ± 4°—which is not significant from a structural perspective. The calculated relative total energies ΔE, relative Gibbs free energies ΔG, and the normalized Boltzmann factor B_f at 298.15 K based on the relative total energies and Gibbs free energy, of all the conformers of **3**, are listed in Table 1.

Among all the conformers, the *boat*-like form conformers have been found to be much more stable than the *chair*-like conformers, to the extent that the *boat*-like form conformers completely dominate at room temperature. This is consistent with previous calculations of analogous ring systems, as well as X-ray crystallographic data.[4a,12] All of the six most stable conformers show extensive intramolecular H-bonds, with three or two in each. The OH···N intramolecular H-bonds are in general as strong as or stronger than the OH···O H-bonds, as indicated by their similar or shorter H-bond distances (Fig. 2). It is therefore not surprising that the two most stable conformers, **BIa** and **BIb**, both contain OH···N intramolecular H-bonds. The three most stable conformers: **BIa**, **BIb**, and **BIIa** account for close to 90% of the total conformer population.

Analysis of ECD spectra

The experimental ECD spectra of **3** and **4** are depicted in Fig. 3. As one can see, they are good mirror images of one another, indicating that these two compounds are enantiomers. The two cotton bands observed at 190 and 286 nm are of the same sign, although the intensity of the peak at 190 nm is more than forty times higher than that at 286 nm.

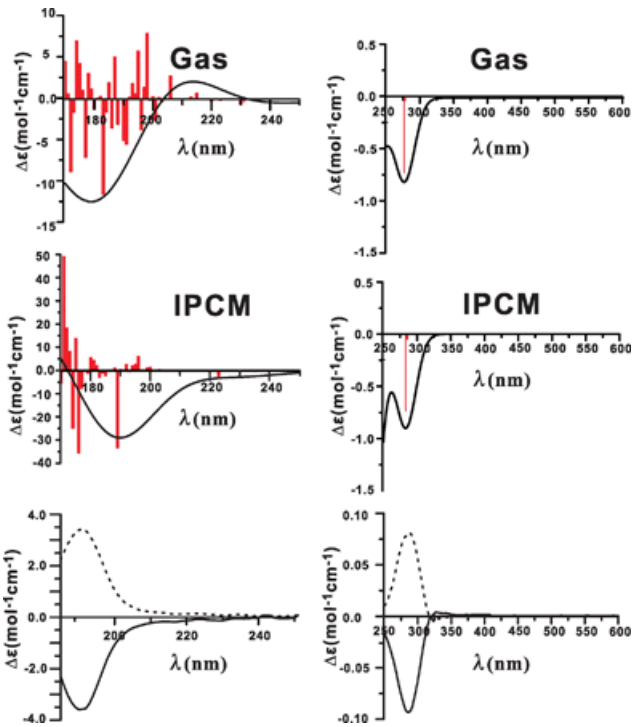

Fig. 3 Comparison of the calculated gas phase and IPCM solution phase ECD spectra of **3** with the experimental (bottom) ECD spectra of **3** (—) and **4** (—) in acetonitrile at 25 °C.

To simulate the ECD spectrum of **3**, the excitation energies, oscillator strengths, and rotational strengths of the 25 lowest energy electronic excitations of the six most stable conformers of **3** have been calculated by using time dependent DFT (TDDFT) at the B3LYP/6-311++G** levels. From these results, we found that the differences between the rotational strengths calculated using the length- and velocity-gauge representation of the electric dipole operator are quite small (Table S2, ESI†), confirming the suitability of the 6-311++G** basis set for this type of calculations. The simulated ECD spectra of the six most stable conformers in the gas phase are given in Figure S2, ESI.† To account for the effects of the acetonitrile solvent, we employed the implicit continuum

polarization model (IPCM). The geometries of the six most stable conformers have been re-optimized and the above ECD spectral calculations repeated under the solution phase IPCM condition. The resulting ECD spectra with IPCM for the six conformers are given in Figure S3, ESI.†

The origin-independent velocity rotational strengths weighted by the conformational populations are plotted in Fig. 3, together with the corresponding population weighted ECD spectra simulated by using a Gaussian band shape[13] with a bandwidth of $\sigma = 0.2$ eV. The gas phase ECD and the IPCM solution ECD spectra look similar, except that the predicted absolute intensity of the IPCM ECD spectrum is considerably higher than that of the gas phase spectrum. In both cases, the simulated ECD spectrum exhibits an intense band at ~190 nm and a weaker band at ~280 nm. Both of these Cotton bands were predicted to have negative signs. The calculated gas phase and IPCM ECD spectra therefore capture not only the band positions but also the relative intensity of the experimental data very well. Consequently, one can unambiguously determine the AC of **3** to be the same as pictured in Chart 1, as assigning it to the opposite enantiomer is clearly unreasonable. The AC of **3** determined directly here is consistent with what was derived indirectly for **3** based on the X-ray structure determination of a crystalline 2,4-dinitrophenylhydrazone derivative of **1**.[5d]

Analysis of ORD spectra

It had been shown that the specific OR values calculated using hybrid-DFT functionals are sensitive to the basis sets used, and aug-cc-pVDZ can, in general, reproduce both the sign and the magnitude of the experimental values.[14] Therefore, the OR values of the six most stable conformers were calculated at the B3LYP/aug-cc-pVDZ level with the B3LYP/6-311++G** optimised geometries reported in the previous section, under both the gas phase and the IPCM solution phase conditions. Comparisons of the population weighted ORD curves with the experimental one are given in Fig. 4. The experimental OR value of **3** becomes more positive as the wavelength increases. Although the magnitude of the OR values have not been predicted exactly, both the sign and the general trend observed experimentally with increasing wavelength have been captured by the simulations. Again, the OR values obtained with the solution phase IPCM calculations are closer to the experimental ones than from the gas phase calculations in our specific case. For a more systematic investigation about how well the IPCM calculations account for the solvent effects in the ECD and ORD measurements, the readers are referred to Ref. 15. Inspection of Fig. 4 shows that the same conclusion can be drawn about the AC of **3** from the ORD study as from the ECD investigation

Although, significant progresses in ORD calculations had been made in the past few years, it is generally acknowledged that the quantitative agreements between experimental and theoretical OR values are still difficult to achieve.[6a,16] For example, even for a simple chiral molecule such as propylene oxide whose OR values are close to zero at some wavelengths, quantitative agreements are nevertheless challenging even with the current state-of-the-art calculations.[17] On the other hand, it is possible to capture both sign and general wavelength variation trend in more favourable cases where the OR values are far away from zero, such as in the present case. Consequently, one can use the results to derive the AC information about the samples.

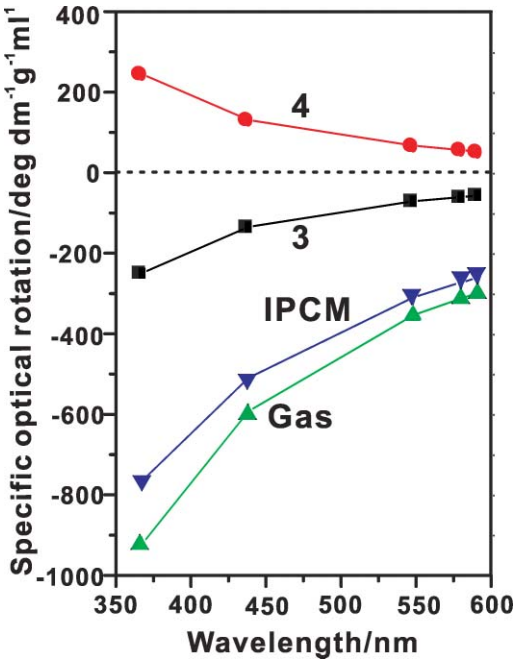

Fig. 4 Comparison of the experimental ORD curves for compounds **3** and **4** with the simulated ORD curves of compound **3** under both the gas phase and solution phase IPCM conditions at the B3LYP/aug-cc-pVDZ level.

Analysis of VA and VCD spectra

It is known that for most monosaccharides, their mid-infrared VCD spectra in the commonly accessible 1000–1800 cm^{-1} region are typically broad and relatively weak, and are often confined to an even smaller region of less than 1500 cm^{-1}.[7] Furthermore, theoretical simulations of the VCD spectra of monosaccharides face serious challenges due to their flexibility and solvent effects. These difficulties had, in the past, hampered efforts to determine ACs of monosaccharides using VCD spectroscopy with DFT calculations, except for a few specifically chosen protected monosaccharide samples that have considerably fewer hydroxyl functional groups.[7] In the present case, although a good number of conformers have been identified, the six most stable conformers account for already ~93% of the total population and three most stable ones for close to 90%. With this smaller number of dominant conformers, it may be possible to confidently identify spectrum—structure relationships by inspecting the VA and VCD spectra of each conformer and then comparing them with the experimentally observed spectra.

The harmonic vibrational frequencies, dipole strengths, and rotational strengths of the six most stable conformations (Fig. 2) have been calculated at the B3LYP/6-311++G** level and their corresponding VA and VCD spectra are shown in Fig. 5. To evaluate the influence of basis sets on the calculated VA and particularly on the VCD spectra, we also used the aug-cc-pVDZ basis set to re-optimize these six most stable conformers and to re-calculate their VA and VCD spectra. The population weighted VA and VCD spectra using these two different basis sets are

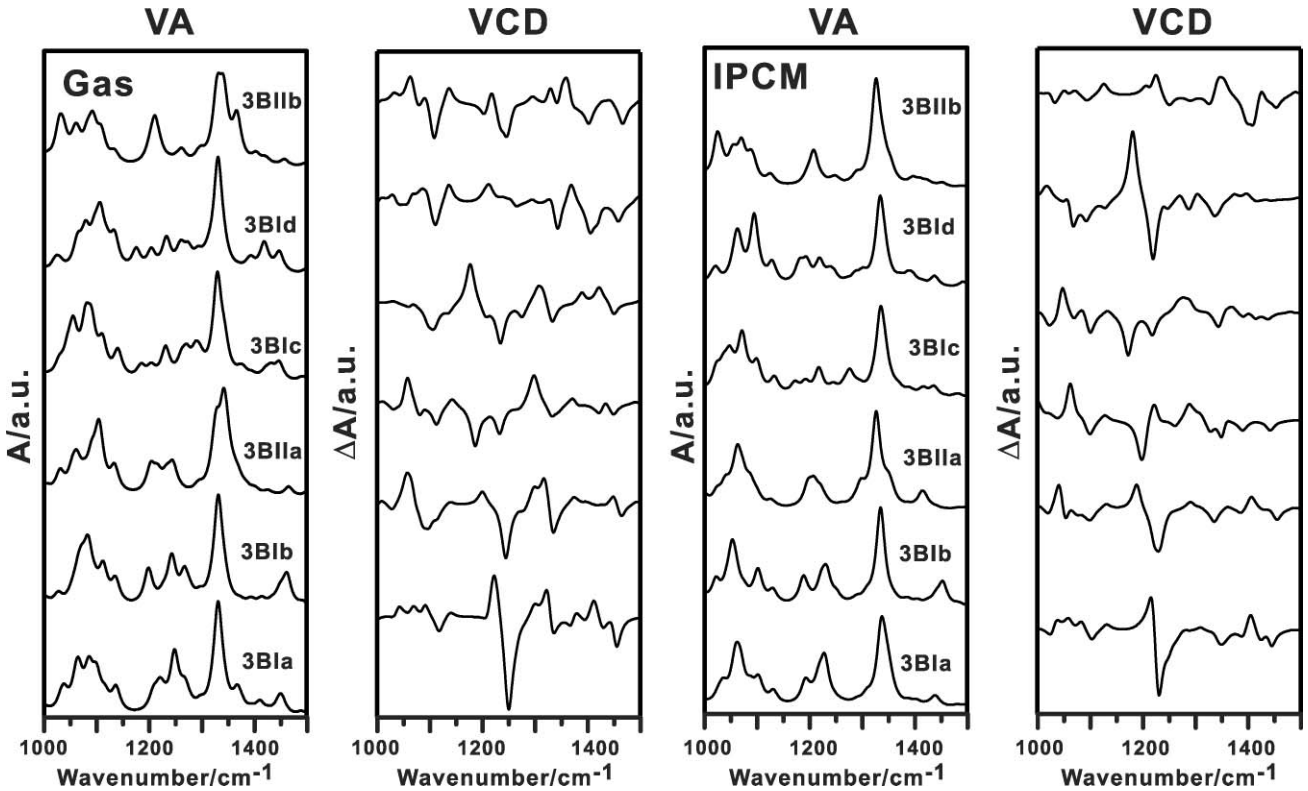

Fig. 5 The gas phase and the solution phase IPCM simulations of the VA and VCD spectra of the six most stable conformers of **3** at the B3LYP/6-311++G** level of theory.

summarized in Figure S4 in the ESI.† As one can see, the differences between the simulated VA and VCD spectra using these two different basis sets are small. To account for the solvent effects, acetonitrile-d_3 was treated as a continuum dielectric environment as in the previous ECD and ORD analyses, and the geometry optimizations and the spectral simulations of the six most stable conformers were repeated with IPCM at the B3LYP/6-311++G** level. The VA and VCD spectra of the six most stable conformers obtained with the IPCM consideration for these conformers are also given Fig. 5 for comparison. The spectra simulated with IPCM show noticeable shifts in some peak frequencies and small changes in some peak intensities when compared to the corresponding gas phase ones.

Finally, the population weighted VA and VCD spectra of the six most stable conformers based on the gas phase and the IPCM solution simulations were compared to the experimental spectra as shown in Fig. 6. The overall agreement of the predicted and experimental VA, especially that of the VCD spectra, supports the same assignment of the AC of **3** as obtained above with the ECD and ORD methods. In the population weighted VA spectra, the VA peak at ~1330 cm^{-1} was predicted to be much stronger than was observed experimentally. This is because the particular peak frequency was predicted to be more or less the same for all six conformers, resulting in a strong intensity enhancement in the population weighted spectrum. It is also noted that in general the agreement with the experimental data improves slightly with the IPCM consideration of the solvent effects. Similar improvements had been reported previously for the study of fenchone, camphor,

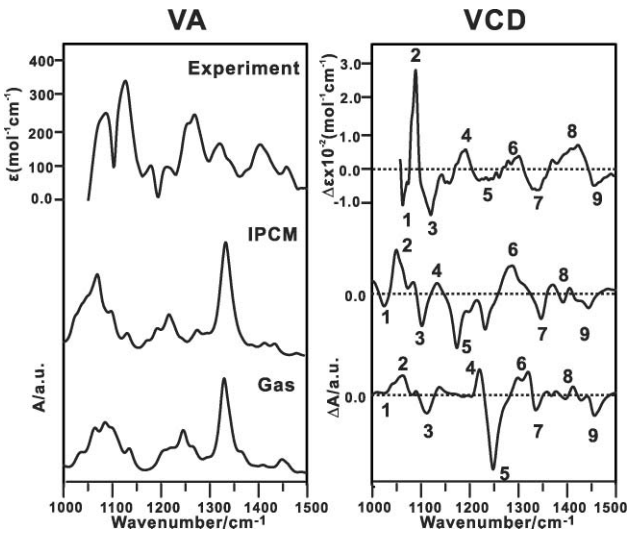

Fig. 6 Comparison of the experimental VA and VCD spectra of **3** with the corresponding population weighted spectra of **3** based on the gas phase and the solution phase IPCM simulations.

α-pinene, β-pinene, camphorquinone, verbenone, and methyloxirane in a number of common solvents such as cyclohexane, acetone, methanol, and acetonitrile.[18] The same conclusion about the inclusion of IPCM was obtained here and in our ECD and ORD analyses discussed above.

Conclusion

In this report, the ACs of **3** and **4**, a pair of enantiomers of a bicyclo[3.1.0]hexane derivative, have been reliably determined by means of three chiroptical methods, namely ECD, ORD, and VCD spectroscopy, in combination with the DFT simulations. Extensive conformational searches for compound **3** have been carried, where the *boat*-like bicyclo[3.1.0]hexane ring conformers have been found to be much more stable than the *chair*-like conformers, and intramolecular H-bonds play a dominant role in the relative conformational stability. In addition, the inclusion of solvent effects by using the IPCM model in the simulations has provided better agreements with the experimental spectra. This example shows that the application of multiple chiroptical spectroscopic methods in combination with DFT theoretical calculations can be successfully applied to reliably determine the ACs of carbohydrates analogs with a large amount of conformational freedom. Such approaches are of great potential use in situations where obtaining an X-ray crystal structure of the molecule is impossible due to problems in crystallization the molecule, or its derivatives.

Experimental and computational details

The synthesis of **3** and **4** used in this study was described previously.[5d] ECD spectra of **3** and **4** were recorded at 25 °C, from 600–185 nm, on an *OLIS DSM* 17 circular dichroism instrument using a 1 mm (Hellma) cuvette. A cell with a path length of 0.2 mm and a sample of 2.5 mg ml^{-1} concentration in acetonitrile were used for the measurements between 185 nm and 250 nm. Another cell with a path length of 1 mm and a concentration of 12.5 mg ml^{-1} in acetonitrile were used for the measurements between 250 nm and 600 nm. Prior to each sample measurement, the cuvette was rinsed three times with dry acetonitrile, and then rinsed three times with the sample solution. Three replicates were recorded, and then averaged and smoothed with *OLIS Globalworks* to produce the final spectrum. Acetonitrile background spectrum was recorded under the same conditions and was subtracted from each sample spectrum. Spectral units are expressed in molar extinction, $\Delta\varepsilon$ ($M^{-1}cm^{-1}$).

The OR values of **3** and **4** at five discrete wavelengths, *i.e.* 589, 578, 546, 436, and 365 nm, were measured with a sample concentration of 0.2 M in acetonitrile using a PERKIN-ELMER 241 polarimeter. **3** and **4** show identical OR magnitudes but with opposite signs (Fig. 4) within the experimental uncertainty.

The VA and VCD spectra were recorded with a Fourier transform IR spectrometer Vertex 70 (Bruker) equipped with a PMA 50 (Bruker) VCD optical bench. Samples were held in a variable path length cell with BaF_2 windows. A frequency filter with a cutoff at ~1800 cm^{-1} was inserted into the beam path right before the photoelastic modulator. The spectral range of the measurements is from 1050 to 1800 cm^{-1}. Each VCD spectrum was collected with a total acquisition time of 180 min (3 × 60 min) and with a resolution of 4 cm^{-1}. An optimal experimental condition with a sample of ~0.2 M in acetonitrile-d_3 and a path length of 100 μm was determined to keep the absorption coefficients of most of the VA peaks in the measured frequency region between 0.2 and 0.8. This helped to minimize artefacts in the VCD measurements. The raw VCD spectra of **3** and **4** are given in Figure S5, as ESI.† The VA spectrum was obtained by subtracting the corresponding solvent spectrum recorded under the same conditions from the solution spectrum, whereas the VCD spectrum was obtained by subtracting the spectrum of **3** from that of **4** under the identical conditions and then dividing it by 2.

The geometry optimizations, vibrational frequencies, and VCD intensities for the conformers of **3** have been performed using the Gaussian03 program package.[19] In this study, the B3LYP[20,21] hybrid functional has been chosen because of its proven reliability in predicting VCD intensities and geometries.[8,22–24] The local minima of **3** were optimized using the 6-311++G** basis set on all atoms. The TDDFT methods as implemented in the Gaussian 03 package were utilized for the OR and ECD calculations.[25] Lorentzian line shapes with a full width at half maximum (FWHM) of 10 cm^{-1} were used to simulate the VA and VCD spectra. Gaussian bandshapes[26] with a bandwidth σ of 0.2 eV were used to simulate the ECD spectra. To evaluate the solvent effects due to acetonitrile, the integral equation formalism (IEF)[27] version of the PCM[28] as implemented in Gaussian03 was utilized. The acetonitrile solvent was treated as a continuum dielectric environment with a dielectric constant of 36.64. The solution VA, VCD, ECD, and ORD spectra were simulated with the inclusion the acetonitrile solvent using the IPCM method.

Acknowledgements

This research was funded by the University of Alberta, the Natural Sciences and Engineering Research Council of Canada, Alberta Ingenuity, the Alberta Ingenuity Centre for Carbohydrate Science, and Petro-Canada. J. L. thanks the Alberta Heritage Foundation for Medical Research for a Studentship. We thank W. Moffat for the electronic circular dichroism and optical rotation measurements and Michele R. Richards for technical assistance. We also gratefully acknowledge access to the computing facilities provided by the Academic Information and Communication Technology group at the University of Alberta.

References

1 (*a*) T. L. Lowary, *Glycoscience: Chemistry and Chemical Biology*, 2001, 2005–2080; (*b*) P. J. Brennan and H. Nikaido, *Annu. Rev. Biochem.*, 1995, **64**, 29–63; (*c*) D. Chatterjee, *Curr. Opin. Chem. Biol.*, 1997, **1**, 579–588; (*d*) P. J. Brennan, *Tuberculosis*, 2003, **83**, 91–97.
2 (*a*) S. Berg, D. Kaur, M. Jackson and P. J. Brennan, *Glycobiology*, 2007, **17**, 35R–56R; (*b*) C. E. I. Barry and K. Mdluli, *Trends Microbiol.*, 1996, **4**, 275–281.
3 C. Altona and M. Sundaralingam, *J. Am. Chem. Soc.*, 1972, **94**, 8205–8212.
4 (*a*) V. E. Marquez, *The Properties of Locked Methanocarba Nucleosides in Biochemistry, Biotechnology, and Medicinal Chemistry in Modified Nucleosides: in Biochemistry, Biotechnology and Medicine*, ed. P. Herewijn, 2008, Wiley-VCH Verlag GmbH & Co. KGaA, p. 305–341; (*b*) M. Meldgaard and J. Wengel, *J. Chem. Soc., Perkin Trans. 1*, 2000, 3539–3554.
5 (*a*) T. L. Lowary, *Mini-Rev. Med. Chem.*, 2003, **3**, 689–707; (*b*) R. Lucas, P. Balbuena, J. C. Errey, M. A. Squire, S. S. Gurcha, M. McNeil, G. D. Besra and B. G. Davis, *ChemBioChem*, 2008, **9**, 2197–2199; (*c*) J. Li and T. L. Lowary, *Org. Lett.*, 2008, **10**, 881–884; (*d*) J. Li, T. L. Lowary and R. McDonald, *Acta. Crystallogr. Sect. E*, 2008, **64**, o459–o460.
6 (*a*) T. D. Crawford, *Theor. Chem. Acc.*, 2006, **115**, 227–245; (*b*) S. Superchi, E. Giorgio and C. Rosini, *Chirality*, 2004, **16**, 422–451; (*c*) T. B. Freedman, X. Cao, R. K. Dukor and L. A. Nae, *Chirality*, 2003, **15**, 743–758; (*d*) P. J. Stephens, F. J. Devlin, C. S. Ashvar, C. F. Chabalowski and M. J. Frisch, *Faraday Discuss.*, 1994, **99**, 103–119; (*e*) L. D. Barron, *Molecular light scattering and optical activity*, 2nd ed. Cambridge Univ Press 2004; (*f*) T. Brotin, D. Cavagnat, J. P. Dutasta

and T. Buffeteau, *J. Am. Chem. Soc.*, 2006, **128**, 5533–5536; (*g*) S. Allenmark and J. Gawronski, *Chirality*, 2008, **20**, 606–608; (*h*) P. J. Stephens, J. J. Pan, F. J. Devlin, M. Urbanova, O. Julinek and J. Hajicek, *Chirality*, 2008, **20**, 454–470.
7 T. Taniguchi and K. Monde, *Chem.–Asian J.*, 2007, **2**, 1258–1266.
8 P. L. Polavarapu, *Chirality*, 2008, **20**, 664–672.
9 (*a*) J. C. Rees and D. Whittaker, *Org. Magn. Reson.*, 1981, **15**, 363–369; (*b*) P. Kang, J. Choo, M. Jeong and Y. Kwon, *J. Mol. Struct.*, 2000, **519**, 75–84; (*c*) T. Kuppens, K. Vandyck, J. Van der Eycken, W. Herrebout, B. J. van der Veken and P. Bultinck, *J. Org. Chem.*, 2005, **70**, 9103–9114.
10 (*a*) T. Buffeteau, D. Cavagnat, A. Bouchet and T. Brotin, *J. Phys. Chem. A*, 2007, **111**, 1045–1051; (*b*) W. Q. Sun, J. Wu, B. Zheng, Y. J. Zhu and C. B. Liu, *THEOCHEM*, 2007, **809**, 161–169; (*c*) K. Nakao, Y. Kyogoku and H. Sugeta, *Faraday Discuss.*, 1994, **99**, 77–85; (*d*) P. Zhang and P. L. Polavarapu, *J. Phys. Chem. A*, 2007, **111**, 858–871; (*e*) T. Kuppens, W. Herrebout, B. von der Veken and P. Bultinck, *J. Phys. Chem. A*, 2006, **110**, 10191–10200.
11 C. Altona and M. Sundaralingam, *J. Am. Chem. Soc.*, 1972, **94**, 8205–8212.
12 (*a*) C. S. Callam, R. R. Gadikota and T. L. Lowary, *J. Org. Chem.*, 2001, **66**, 4549–4558; (*b*) L. H. Koole, S. Neidle, M. D. Crawford, A. A. Krayevski, G. V. Gurskaya, A. Sandström, J.-C. Wu, W. Tong and J. Chattopadhyaya, *J. Org. Chem.*, 1991, **56**, 6884–6892.
13 D. M. McCann and P. J. Stephens, *J. Org. Chem.*, 2006, **71**, 6074–6098.
14 (*a*) J. R. Cheeseman, M. J. Frisch, F. J. Devlin and P. J. Stephens, *J. Phys. Chem. A*, 2000, **104**, 1039–1046; (*b*) K. B. Wiberg, *J. Comput. Chem.*, 2004, **25**, 1342–1346; (*c*) P. J. Stephens, D. M. McCann, J. R. Cheeseman and M. J. Frisch, *Chirality*, 2005, **17**, S52–S64; (*d*) M. D. Kundrat and J. Autschbach, *J. Phys. Chem. A*, 2006, **110**, 4115–4123; (*e*) B. Mennucci, M. Claps, A. Evidente and C. Rosini, *J. Org. Chem.*, 2007, **72**, 6680–6691.
15 M. Pecul, D. Marchesana, K. Ruud and S. Coriani, *J. Chem. Phys.*, 2005, **122**, 024106.
16 P. Mukopadhyay, P. Wipf and D. N. Beratan, *Acc. Chem. Res.*, 2009, **42**, 809–819.
17 (*a*) S. M. Wilson, K. B. Wiberg, J. R. Cheeseman, M. J. Frisch and P. H. Vaccaro, *J. Phys. Chem. A*, 2005, **109**, 11752–11764; (*b*) M. Losada, P. Nyguen and Y. Xu, *J. Phys. Chem. A*, 2008, **112**, 5621–5623; (*c*) K. Ruud and R. Zanasi, *Angew. Chem., Int. Ed.*, 2005, **44**, 3594–3596.
18 B. Mennucci, J. Tomasi, R. Cammi, J. R. Cheeseman, M. J. Frisch, F. J. Devlin, S. Gabriel and P. J. Stephens, *J. Phys. Chem. A*, 2002, **106**, 6102–6113.
19 M. J. Frisch *et al.* Gaussian 03 (Revision C.02): see Supporting Information.
20 A. D. Becke, *J. Chem. Phys.*, 1993, **98**, 5648–5652.
21 C. T. Lee, W. T. Yang and R. G. Parr, *Phys. Rev. B: Condens. Matter*, 1988, **37**, 785–789.
22 (*a*) P. J. Stephens, F. J. Devlin, C. F. Chabalowski and M. J. Frisch, *J. Phys. Chem.*, 1994, **98**, 11623–11627; (*b*) P. J. Stephens, F. J. Devlin and J. J. Pan, *Chirality*, 2008, **20**, 643–663.
23 (*a*) M. Losada and Y. Xu, *Phys. Chem. Chem. Phys.*, 2007, **9**, 3127–3135; (*b*) M. Losada, H. Tran and Y. Xu, *J. Chem. Phys.*, 2008, **128**, 014508; (*c*) G. Yang and Y. Xu, *J. Chem. Phys.*, 2009, **130**, 164506; (*d*) G. Yang, Y. Xu, J. Hou, H. Zhang and Y. Zhao, *Chem.–Eur. J.*, 2010, **16**, 2518, DOI: 10.1002/chem.200902501; (*e*) G. Yang and Y. Xu, *Phys. Chem. Chem. Phys.*, 2008, **10**, 6787–6795.
24 L. Ducasse, F. Castet, A. Fritsch, I. Huc and T. Buffeteau, *J. Phys. Chem. A*, 2007, **111**, 5092–5098.
25 (*a*) J. R. Cheeseman, M. J. Frisch, F. J. Devlin and P. J. Stephens, *J. Phys. Chem. A*, 2000, **104**, 1039–1046; (*b*) J. Autschbach, T. Ziegler, S. J. A. van Gisbergen and E. J. Baerends, *J. Chem. Phys.*, 2002, **116**, 6930–6940.
26 D. M. McCann and P. J. Stephens, *J. Org. Chem.*, 2006, **71**, 6074–6098.
27 E. Cancès, B. Mennucci and J. Tomasi, *J. Chem. Phys.*, 1997, **107**, 3032–3041.
28 (*a*) J. Tomasi and M. Persico, *Chem. Rev.*, 1994, **94**, 2027–2094; (*b*) C. Cramer and D. Truhlar, *Chem. Rev.*, 1999, **99**, 2161–2200.